Thermal stability of interstitial and substitutional Mn in ferromagnetic (Ga,Mn)As

T. A. L. Lima,[1] U. Wahl,[1,2] A. Costa,[2] V. Augustyns,[1] K. W. Edmonds,[3]
B. L. Gallagher,[3] R. P. Campion,[3] J. P. Araújo,[4] J. G. Correia,[2]
M. R. da Silva,[2] K. Temst,[1] A. Vantomme,[1] and L. M. C. Pereira[1, *]

[1]*KU Leuven, Instituut voor Kern- en Stralingsfysica, 3001 Leuven, Belgium*

[2]*Centro de Ciências e Tecnologias Nucleares, Instituto Superior Técnico,*
Universidade de Lisboa, 2686-953 Sacavém, Portugal

[3]*School of Physics and Astronomy, University of Nottingham,*
Nottingham NG7 2RD, United Kingdom

[4]*IFIMUP and IN-Institute of Nanoscience and Nanotechnology,*
Universidade do Porto, 4169-007 Porto, Portugal

(Dated: August 23, 2019)

Abstract

In (Ga,Mn)As, a model dilute magnetic semiconductor, the electric and magnetic properties are strongly influenced by the lattice sites occupied by the Mn atoms. In particular, the highest Curie temperatures are achieved upon thermal annealing in a narrow temperature window around $200°C$, by promoting the diffusion of interstitial Mn towards the surface. In this work, we determined the thermal stability of both interstitial and substitutional Mn in ferromagnetic (Ga,Mn)As thin films, using the emission channeling technique. At a higher Mn concentration, the temperatures at which substitutional and interstitial Mn become mobile not only decrease, but also become closer to each other. These findings advance our understanding of self-compensation in (Ga,Mn)As by showing that the strong dependence of the Curie temperature on annealing temperature around $200°C$ is a consequence of balance between diffusion of interstitial Mn and segregation of substitutional Mn.

I. INTRODUCTION

(Ga,Mn)As, a dilute magnetic semiconductor (DMS), is a model system for studying carrier-mediated ferromagnetism in semiconductors and the associated spintronic phenomena.[1–3] In ferromagnetic (Ga,Mn)As thin films, which are typically grown by low-temperature molecular beam epitaxy (LT-MBE), Mn atoms mainly occupy Ga sites with a minority fraction occupying interstitial sites.[4–6] Substitutional Mn atoms (Mn_s) provide both the localized magnetic moment and the itinerant holes that mediate the magnetic coupling. On the other hand, interstitial Mn atoms (Mn_i) have a doubly compensating effect: magnetic compensation since Mn_i couple antiferromagnetically with Mn_s; electric compensation since Mn_i are double donors.[5] At a given Mn concentration, the substitutional-to-interstitial ratio strongly influences the hole concentration, the Fermi level, and the effective magnetization provided by non-compensated Mn_s moments.[1–7]

Previous studies on (Ga,Mn)As have focused on a careful optimization of the synthesis and post-growth treatments, aiming to improve two key properties: the Curie temperature (T_C) and the magnetization.[4–8] In these studies at high Mn concentration (several percent), interstitial Mn was found to out-diffuse during thermal annealing in the 160°C-200°C temperature range.[7–10] The highest T_C in (Ga,Mn)As (188 K) has been achieved for a Mn concentration of ∼12% after growth at low temperature ($T_G \sim 200$°C), followed by thermal annealing in air at 160°C.[7,8] Understanding the diffusion of interstitial Mn (i.e. its thermal stability) is crucial, as it defines the lower limit for the optimum annealing temperature window. In particular, the binding energy of the interstitial Mn in complexes such as Mn_s-Mn_i pairs and Mn_s-Mn_i-Mn_s triplets,[11,12] which can be as high as 0.8 eV,[10,13] contributes to its thermal stability. Therefore, since the fraction of Mn atoms in Mn_s-Mn_i pairs is expected to increase with increasing Mn concentration, so would the thermal stability of *interstitial* Mn. However this dependence has not been studied so far. On the other hand, the diffusion and segregation of *substitutional* Mn also plays a central role on the magnetic properties of (Ga,Mn)As, as it defines the upper limit for optimum annealing. Experiments based on ion channeling showed that part of the substitutional Mn is converted to a non-substitutional (random) component at annealing temperatures as low as ∼ 280°C.[6] Additionally, a detailed study of the dependence of T_C on annealing temperature revealed a decrease in T_C with increasing annealing temperature in the range 160-220°C, suggesting an onset of segregation of

Mn$_s$.[9] However, these temperatures are well below the well-understood regime of secondary phase formation (>400°C).[11,12,14,15] Moreover, direct evidence for Mn$_s$ segregation around 200°C is still lacking.

The diffusion of interstitial Mn and the segregation of substitutional Mn in (Ga,Mn)As remain poorly understood. In this paper, we address this gap in understanding gap by studying the thermal stability of Mn in ferromagnetic (Ga,Mn)As with a concentration of 1% and 5%. Using the emission channeling technique, we observe that, with increasing Mn concentration, the temperatures at which Mn$_s$ and Mn$_i$ become mobile not only decrease, but also become closer to each other. These results show that the narrow annealing temperature window in which the T_C and magnetization can be optimized in (Ga,Mn)As results from a fine balance between diffusion of Mn$_i$ and segregation of Mn$_s$.

II.   EXPERIMENTAL DETAILS

The emission channeling technique makes use of charged particles emitted by a decaying radioactive isotope, usually β^- decay electrons or conversion electrons.[16] These particles are emitted isotropically during decay and are channeled along the screened Coulomb potential of atomic rows and planes. Along low-index crystal directions of single crystals or epilayers, this anisotropic scattering results in well-defined channeling or blocking effects. Because these effects strongly depend on the initial position of the emitted particles, they produce emission patterns which are characteristic of the lattice sites occupied by the probe atoms. Emission channeling experiments were performed by implanting a low concentration (< 0.05%) of radioactive ^{56}Mn (half-life $t_{1/2}$ = 2.56 h) or ^{73}As (half-life $t_{1/2}$ = 80 d) into (Ga,Mn)As thin films. Angular-dependent emission patterns are recorded along various crystallographic axes using a position- and energy-sensitive detection system similar to that described in Ref. 17. The theoretical emission patterns for probes occupying a large variety of possible lattice sites are calculated using the *manybeam* formalism for electron channeling in single crystals.[16] Quantitative lattice location is provided by fitting the experimental patterns with theoretical ones using a two-dimensional fit procedure.[18] Corrections for backscattered electrons that reach the detector were implemented by subtracting an isotropic background from every pattern. This backscattered electron contribution is estimated based on Geant4 simulations of electron scattering,[19,20] taking into account the elemental composition and

sample	[Mn]	t [nm]	isotope	E [keV]	R_p [nm]	σ [nm]	x_p [cm^{-3}]	fluence [cm^{-2}]	θ [°]
A	1%	1500	^{56}Mn	30	21	11	2.4×10^{18}	7×10^{12}	17
B	5%	200	^{56}Mn	30	21	11	2.4×10^{18}	7×10^{12}	17
C	5%	200	^{73}As	50	26	13	1.5×10^{19}	5×10^{13}	10

TABLE I. Sample and implantation details. All implantations were performed at room temperature. The peak concentrations (x_p), projected ion range (R_p) and straggling (σ) were estimated using SRIM-2008 code.[21]. The sample thickness, implantation energy and angle are denoted, respectively, by t, E and θ.

geometry of the sample, sample holder and vacuum chamber. By probing the site occupancy of the radioactive probes as a function of annealing temperature we can investigate their thermal stability.

To this purpose a series of emission channeling experiments were performed on (Ga,Mn)As films, grown using low temperature molecular beam epitaxy, as described in Refs. 8 and 22. The samples and experimental details are given in Table I. The quoted Mn concentrations ([Mn]) are estimated values based on a series of calibration measurements,[23] and correspond to a density of $2.2x \times 10^{20}$ cm^{-3}, where x is the quoted [Mn]. The results from sample A and B can be directly compared regarding the thermal stability of ^{56}Mn in (Ga,Mn)As with two different concentrations. The ^{73}As experiment, on sample C, was performed to probe the stability of the GaAs host lattice when annealing up to high temperatures ($\sim 600°$C). All implantations were performed at room temperature and subsequent measurements were carried out in the as-implanted state and after thermal annealing in steps of 50°C (100°C for the ^{73}As experiment) starting at 100°C. Each annealing step was performed in high vacuum ($< 10^{-5}$ mbar) for 10 min. Angular-dependent emission patterns were recorded along four crystallographic axes ($\langle 100 \rangle$, $\langle 111 \rangle$, $\langle 110 \rangle$ and $\langle 211 \rangle$) at room temperature.

III. RESULTS AND DISCUSSION

Emission channeling results are presented and discussed in two parts starting with the identification of which lattice sites Mn occupies in (Ga,Mn)As (section III A), followed by the analysis of Mn diffusion and thermal stability for both Mn concentrations (section III B). This analysis includes a model for the diffusion of both Mn_s and Mn_i, as well as a discussion of its implications on the understanding of Mn thermal stability in (Ga,Mn)As.
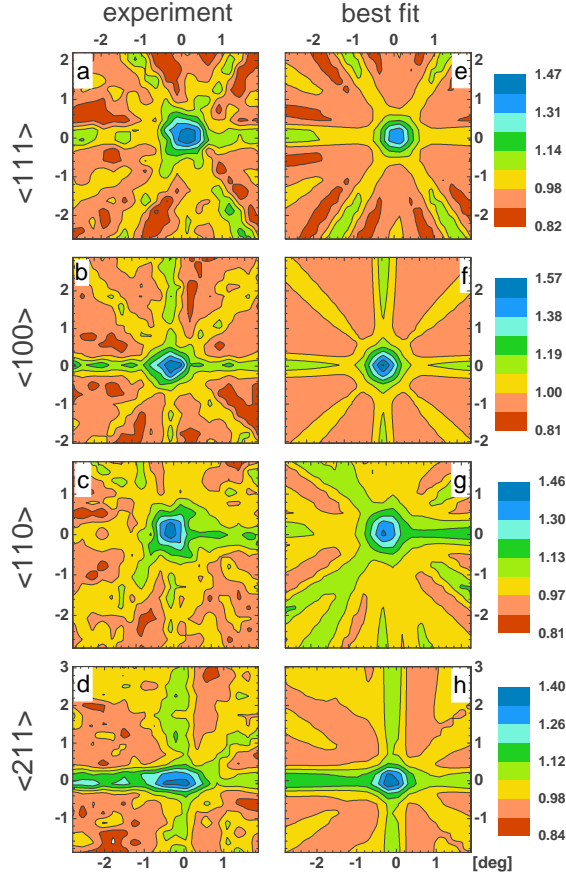
FIG. 1. (a)-(d) Normalized experimental ^{56}Mn emission channeling patterns in the vicinity of the $\langle 111 \rangle$, $\langle 100 \rangle$, $\langle 110 \rangle$ and $\langle 211 \rangle$ directions of the (Ga,Mn)As film with 5% Mn, following annealing at 350°C. (e)-(h) Corresponding best fits. Fit results averaged over $\langle 110 \rangle$ and $\langle 211 \rangle$ directions yield 65% and 14% of the Mn atoms on S_{Ga} and T_{As} sites, respectively.

A.   Identification of the occupied lattice sites

In (Ga,Mn)As the Mn dopants occupy mainly Ga-substitutional sites S_{Ga}. Fitting calculated S_{Ga} patterns to our experimental results gives by far the best agreement. By including in the fitting tetrahedral interstitial sites with As closest neighbors (T_{As}), the best fit was observed for the $S_{Ga}+T_{As}$ double occupancy patterns, with larger fractions of ^{56}Mn probes occupying the S_{Ga} sites and smaller fractions the T_{As} sites. This is consistent with previous emission channeling experiments showing that interstitial Mn occupies only the T_{As} site, with $< 0.5\%$ of Mn occupying T_{Ga} sites.[24]

As an example of the good match between experiment and simulated patterns, Fig. 1 compares the normalized experimental β^- emission yields for the ^{56}Mn experiment on sample

A, after an annealing step at a temperature of 350°C, along the four measured directions (a-d) with the best fits to theoretical patterns (e-h). Site fractions for the best fit, averaged over $\langle 110 \rangle$ and $\langle 211 \rangle$ directions, give 65% of the ^{56}Mn atoms in S_{Ga} sites and 14% in T_{As} sites. For the radioactive ^{73}As experiment in sample C, the probes were found to occupy exclusively substitutional S_{As} sites, with a site fraction of $\approx 100\%$. Further details are given in the supplementary information.[25] For all experiments presented in Table I, fractions of other possible interstitial sites are estimated to be below 5%, i.e. below the measurement uncertainty.

B. Thermal stability of interstitial and substitutional Mn

Associated with each site is its occupancy, i.e. the fraction incorporated in the respective site with respect to all the implanted ^{56}Mn (or ^{73}As). Site fractions associated with the stable isotopes incorporated during growth will most likely differ, since the kinetics of implantation is very different from that of doping during LT-MBE growth. Once the Mn atoms are at rest their behavior does not depend on their history or isotope, and although the absolute site fractions may differ, the diffusion behavior we investigate here is accurately reproduced by the ^{56}Mn probes. Performing this experiment after several annealing steps provides information on the thermal stability of the occupied lattice sites.

Figure 2(a) shows the results from emission channeling experiments performed on samples A, B, and C, as a function of annealing temperature in comparison with the ultra-dilute case investigated in Ref. 26 (Fig. 2(b)). For each experiment the fitted fractions of ^{56}Mn or ^{73}As probes are plotted for the corresponding lattice sites they occupy, S_{Ga} and T_{As} for ^{56}Mn, and S_{As} for ^{73}As.

In emission channeling experiments, and in particular for (Ga,Mn)As thin films, two phenomena may induce changes in the obtained site fractions: (i) the annealing of implantation induced damage, and (ii) diffusion processes of the implanted probes. The first scenario (i) is observed in (Ga,Mn)As at relatively low annealing temperatures, and while the thermal energy is not sufficient to induce diffusion of Mn atoms, it induces crystalline recovery. In other words, during implantation many defects are created, such as Ga and As vacancies (V_{Ga} and V_{As}) and disordered regions, where radioactive ^{56}Mn probes may become trapped. Probes trapped in these regions emit electrons which will not be channeled due to the irreg-
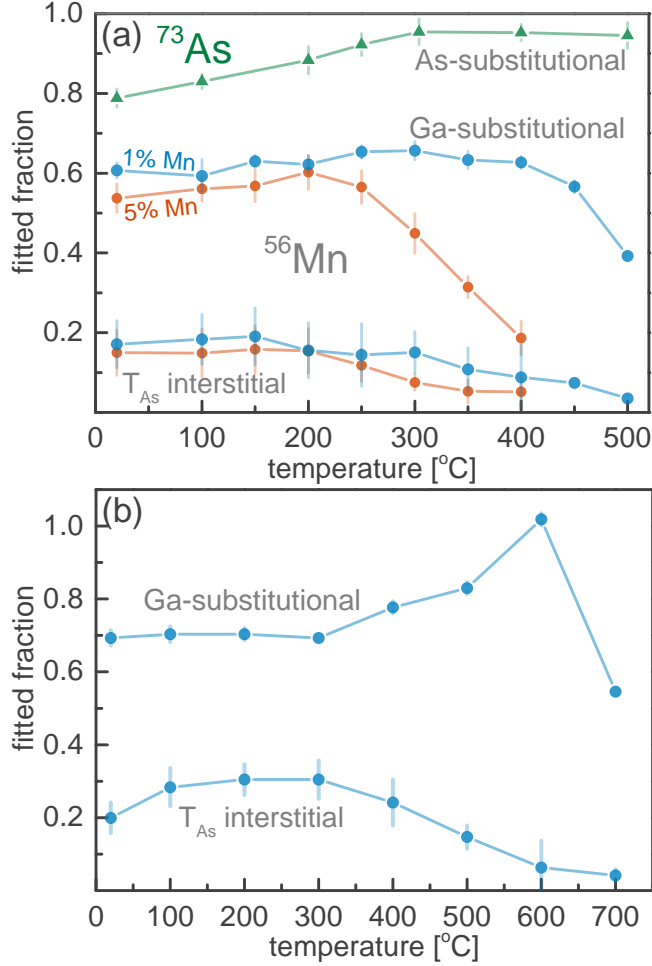
FIG. 2. (a) Fitted fractions of implanted ^{73}As (green triangles) and ^{56}Mn (blue and orange circles) probes on (Ga,Mn)As samples doped with different concentrations of Mn, averaged over the $\langle 110 \rangle$ and $\langle 211 \rangle$ directions. (b) Fitted fractions of implanted ^{56}Mn probes on semi-insulating GaAs, extracted from Ref. 26.

ular potential surrounding them and will reach the detector with an isotropic distribution. On the other hand, radioactive probes can also combine with vacancies (V_{Ga} or V_{As}), contributing to an increase in substitutional site fractions. Annealing of implantation damage is visible in Fig. 2(a), where substitutional fractions increase with increasing annealing temperatures up to 300°C, particularly noticeable in the ^{73}As experiment where the S_{As} fitted fraction increases to near 100%. The second phenomenon (ii), the diffusion of implanted probes, may influence site fractions via two separate mechanisms. On the one hand, once radioactive probes become mobile and diffuse away from their initial position in the sample, this may lead to their incorporation in a different type of lattice site. This has been observed for instance for ^{56}Mn implanted into pure GaAs[26,27] (cf. Fig. 2(b)), where the onset of the

migration of interstitial $^{56}\text{Mn}_\text{i}$ leads to its incorporation in substitutional Ga sites as $^{56}\text{Mn}_\text{s}$ via the combination with Ga vacancies. On the other hand, diffusion also leads to changes in the depth profile of the implanted probes. In that respect, although diffusion occurs in every direction within the film, due to the nature of emission channeling only diffusion towards the surface or deeper into the sample will have an impact on the measured fractions. Electrons emitted from deeper within the sample (diffusion to the bulk) are subjected to stronger dechanneling effects, whereas electrons emitted from the first few atomic layers (diffusion towards the surface) do not experience channeling effects. In both cases electrons reach the detector as an isotropic contribution resulting in a decrease in the fitted fractions. We discuss this effect in more detail below, in the context of a Mn diffusion model.

Comparing the ^{56}Mn site fractions to our previous studies in pure GaAs, in Fig. 2(b), one can observe that no pronounced ^{56}Mn site changes from interstitial to substitutional sites are observed in (Ga,Mn)As. In GaAs, a decrease in interstitial ^{56}Mn fraction was accompanied by a corresponding increase in substitutional fraction. We attribute the absence of this effect to the fact that the (Ga,Mn)As samples are saturated with stable Mn_i, incorporated during growth, which fill essentially all Ga-vacancies created during implantation. Since the concentration of stable Mn_i is orders of magnitude larger than the implanted ^{56}Mn, only a negligible fraction of radioactive ^{56}Mn probes participate in this process, and therefore the site change is not observed for ^{56}Mn. In addition, while in GaAs ^{56}Mn on substitutional Ga sites was completely stable against annealing up to a temperature of 600°C, in (Ga,Mn)As the substitutional fraction starts to decrease at much lower temperatures. Moreover, there is a clear distinction between the experiments performed in samples A (1% Mn) and B (5% Mn), showing that the thermal stability of both substitutional and interstitial sites decreases with Mn concentration.

Ultimately, the difference in temperature at which the Mn on substitutional sites becomes mobile for both samples A and B, represented in Fig. 2, is related to a decrease in thermal stability with increasing Mn concentration. This points to a possible onset of Mn segregation at lower temperatures and as such sets an upper limit for the optimum annealing temperature at which T_C can be maximized in (Ga,Mn)As thin films.

The thermal stability of Mn in (Ga,Mn)As is further addressed in the following paragraphs, with an estimate of the activation energies for diffusion of both Mn_s and Mn_i from the emission channeling results presented above, within an adequate diffusion model.

	substitutional		interstitial	
% Mn	$T_{1/2}$ [°C]	E_a^s [eV]	$T_{1/2}$ [°C]	E_a^i [eV]
0.05	700	2.9	$450 - 550$	$1.7 - 2.3$
1	$500 - 550$	2.4	$350 - 450$	$1.6 - 2.0$
5	$350 - 400$	1.9	$250 - 300$	$1.3 - 1.6$

TABLE II. Estimated activation energies E_a for substitutional and interstitial Mn diffusion in (Ga,Mn)As with different Mn concentrations. $T_{1/2}$ represents the temperature range at which our fitted fractions reduce to $f_0/2$. $T_{1/2}$ is described in more detail in the supplementary information.[25]

1. Diffusion model

Activation energies for Mn diffusion in (Ga,Mn)As can be estimated from emission channeling data by assuming a modified Arrhenius model to describe the changes in site fractions, shown in Fig. 2. The details of this calculation are given in the supplementary information,[25] and the model is described in the remainder of this section. The resulting activation energies for substitutional and interstitial diffusion are presented in Table II for both Mn concentrations in the (Ga,Mn)As under study. Additionally, activation energies for [56]Mn diffusion in GaAs from Ref. 26 are also included for comparison. The main observation from Table II is that the activation energies E_a decrease with increasing Mn concentration, for both substitutional and interstitial Mn. In this section, we discuss this observation in more detail and introduce a model for diffusion of Mn in (Ga,Mn)As.

In the ultra-dilute regime ($< 0.05\%$ Mn), where only the implanted [56]Mn probes contribute to the total Mn concentration in GaAs, Mn_i can be assumed to diffuse as a free, isolated interstitial.[28,29] In other words, the probability for a Mn_i atom to occupy a position near a Mn_s atom is very small, as Mn impurities are far apart in an ultra-dilute system. In this scenario the activation energy for free interstitial diffusion can then be directly related to the *migration energy* E_m, which is the energy barrier between neighboring interstitial sites. Since Mn_i was observed to only occupy T_{As} sites both before and after thermal annealing in ferromagnetic (Ga,Mn)As,[24] E_m can be specifically attributed to the energy barrier between neighboring T_{As} interstitial sites. This scenario implies that T_{Ga} is a higher-energy configuration compared to T_{As}, so that the barrier associated with a $T_{As} \rightarrow T_{Ga}$ jump is larger than the reverse $T_{Ga} \rightarrow T_{As}$. This also implies that at room temperature the $T_{Ga} \rightarrow T_{As}$ barrier is overcome, resulting in the prevalence of T_{As} sites. Thus, we can conclude that intersti-

9

tial diffusion occurs along the path $T_{As} \rightarrow T_{Ga} \rightarrow T_{As}$, depicted in Fig. S2 in supplementary information,[25] and its activation energy is directly linked with E_m, $E_a = E_m$.

In the higher concentration regime investigated in this paper, the interstitial diffusion can not be solely modeled by $E_a = E_m$, as a considerable fraction of the interstitials are trapped by neighboring substitutional Mn, forming pairs (Mn_s–Mn_i) and triplets (Mn_s–Mn_i–Mn_s) (cf. Fig. S2 in supplementary information[25]). These complexes contribute to the activation energy for interstitial diffusion with E_b, an additional energy barrier that Mn_i has to overcome to break the bond with substitutional Mn, resulting in $E_a = E_m + E_b$. Following a purely statistical approach, as described in Ref. 30, i.e. assuming that the substitutional Mn is randomly distributed in the lattice, the fractions of isolated substitutional Mn atoms (x_s) and of pairs of neighbouring substitutional Mn atoms (x_{s-s}) as a function of Mn concentration x can be calculated by: $x_s = (1 - x)^{12}$ and $x_{s-s} = 12x(1 - x)^{18}$. For 1% Mn, this gives $x_s = 0.89$ and $x_{s-s} = 0.10$. For 5%, $x_s = 0.54$ and $x_{s-s} = 0.24$. In other words, the probability of interstitial Mn_i to be trapped by complexes involving more than one substitutional Mn_s is considerably enhanced for [Mn] = 5%. E_b^i can then be described as an energy barrier that is largely determined by the Coulomb interaction between oppositely charged Mn_s and Mn_i defects, and should, intuitively, increase with the number of Mn_s atoms involved in the complex. Density functional theory (DFT) calculations have indeed predicted this effect, with binding energies of $E_b^{pair} = 0.49$ eV for the $Mn_i(T_{As})$–Mn_s bond, and $E_b^{triplet} = 0.81$ eV for Mn_s–$Mn_i(T_{As})$–Mn_s bonds.[13]

Given the statistical prevalence of Mn complexes at higher concentrations, one would expect the activation energy for interstitial diffusion to increase with Mn content. However, the emission channeling results presented here show the contrary, i.e. the activation energy for diffusion of interstitial Mn decreases with Mn concentration (cf. Table II), which clearly points towards an additional diffusion enhancing mechanism. We propose that, while increasing Mn concentration adds a binding contribution to the activation energy for interstitial diffusion, associated with the Coulomb interaction between a single Mn_s and a Mn_i atom, the same Coulomb interaction between the interstitial and more distant Mn_s defects decreases the activation energy by an an amount Δ, thus enhancing diffusion. The Coulomb interaction energy between Mn_s^- and Mn_i^{2+} at a distance of 10 Å can be estimated as $\Delta \approx 0.2$ eV, taking the GaAs dielectric constant (13.2). However, within a distance of 10 Å in a 5% Mn sample there are six Mn_s in the neighborhood of each Mn_i, resulting in

possible potential modifications of $\Delta \approx 1.2$ eV. A similar estimation can be performed for a 1% sample, resulting in an interaction energy of $\Delta \approx 0.8$ eV. These energies can effectively compete with E_b^i, ultimately decreasing the activation energy for interstitial diffusion, $E_a = E_m + E_b - \Delta$.

Comparing values for E_a^i in Table II with E_b^i from Ref. 13, discussed above, suggests that the activation energy for interstitial diffusion E_a^i decreases from the ultra-dilute regime to 5% Mn by $\Delta E_a^i \sim 0.1 - 1.0$ eV, driven essentially by the competing contributions from E_b^i and Δ, assuming a similar E_m. However, E_m requires additional discussion. In the ultra-dilute regime E_a^i is entirely due to E_m ($E_a^i = E_m$), and E_a^i is in fact larger than the values determined here for 1% and 5%. Therefore, E_m may also decrease from the ultra-dilute to the few percent regime. A possible contribution to this decrease is the lattice expansion induced by the Mn doping, i.e. that interstitial Mn experiences a lower migration barrier in a more open lattice, although the increase in lattice constant from the ultra-dilute case to 5% Mn in (Ga,Mn)As layers is only 0.2%.[23]). Nevertheless, even if this decrease affects E_m, it alone cannot explain all the observed changes in E_a^i; in that case, E_a^i would vary by the same amount, which is not observed. In order to explain the additional variation, Δ is required.

The diffusion of substitutional Mn, on the other hand, can be assumed to be of the Frank-Turnbull type, i.e. thermally activated Mn_s first leaves its substitutional lattice site and then diffuses as an interstitial until it encounters the next stable trap, usually a Ga vacancy. At sufficiently high Mn concentrations, also regions with segregated Mn can act as traps. The activation energy for this type of diffusion can be split in two terms, one consisting of the binding energy $E_b(Mn_s)$ of Mn to the substitutional site, the other being the activation energy E_a^i for interstitial diffusion of Mn_i, resulting in a total activation energy of $E_a^s = E_a^i + E_b(Mn_s)$. Note that for this type of diffusion mechanism, an increase or a decrease of the activation energy for interstitial diffusion will also lead to a corresponding effect on the stability of the substitutional Mn species. As established above, Δ drives down the activation energy for interstitial diffusion and, consequently, also for substitutional diffusion, in accordance with the results in Table II.

A different model for the diffusion of Mn in (Ga,Mn)As has been proposed in Refs. 31 and 32, which considers that clustering of Mn occurs via pure substitutional diffusion driven solely by Ga vacancies (V_{Ga}). The weakness of this model is that it neglects the interaction

of Mn interstitials with Ga vacancies, i.e. the fact that interstitial Mn, once it becomes mobile, easily converts to substitutional by filling up existing V_{Ga} (which is associated with an energy gain). The reverse process, i.e. dissociation of Mn_s by becoming interstitial and leaving behind a V_{Ga}, is also possible, though only with higher thermal activation energy, cf. the discussion above. In contrast, it is assumed in Refs. 31 and 32 that Mn interstitials have been completely driven out from the sample before clustering of substitutional Mn atoms starts. Moreover, the substitutional diffusion of Mn is assumed to be the consequence of a rather high concentration of mobile V_{Ga} ($\approx 1 \times 10^{18}$ cm^{-3}), which is not explained by the model itself but given as external input. The assumption that interstitial out-diffusion of Mn in (Ga,Mn)As can be entirely completed before any substitutional diffusion starts is contrary to what we observe in our emission channeling experiments, especially in the 5% Mn sample, where the decrease in interstitial and substitutional Mn fractions takes place in overlapping temperature regimes, i.e. the two processes occur simultaneously, though slower for substitutional Mn.

2. Substitutional Mn diffusion as a limiting factor

The temperature at which substitutional Mn becomes mobile changes from 700°C in the ultra-dilute regime, to $\sim$ 500°C at 1% [Mn], to $\sim$ 350°C at 5% [Mn]. Although the formation of MnAs precipitates is well documented in the 400–600°C temperature range,[11,12,14,15] our data show that this segregation process can already take place at lower temperatures, likely with the formation of disordered Mn-rich regions preceding well-defined secondary phases. This scenario is further supported by the emission channeling data obtained upon re-implanting ^{56}Mn after high temperature annealing (400°C for 5% and 500°C for 1% Mn), i.e. after diffusion of a significant fraction of substitutional Mn. A thorough analysis of this effect is beyond the scope of this paper and is therefore only briefly described in the supplementary information.[25]

At several % Mn, segregation can occur at annealing temperatures as low as 200°C, counteracting the improvement of T_C by removal of interstitials, introducing an upper limit for the optimum annealing temperature. On the other hand, the lower limit is determined by the removal of interstitial Mn. From our results (Table II), the activation energy E_a for interstitial diffusion also decreases with Mn concentration, although less significantly than for

substitutional. The annealing temperature window for T_C and magnetization optimization in (Ga,Mn)As is therefore narrowed and limited by two phenomena which have opposite effects on T_C: interstitial out-diffusion and substitutional low-temperature segregation. Although these two processes are governed by rather close activation energies, it is possible to induce the diffusion of interstitial Mn (with a lower activation energy) while minimizing substitutional segregation, as long as the thermal annealing is sufficiently long and at a suitably low temperature (typically several hours for films ~ 25 nm at temperatures of 160–180°C).[9] In this picture, film thickness also plays an important role. Decreasing the thickness also decreases the diffusion distance required for interstitial Mn to be passivated at the surface. In contrast, the segregation of substitutional Mn is in principle unaffected by a reduction in thickness since the required diffusion length is determined in that case by the (local) Mn concentration. Therefore, thinner films favor passivation of interstitial Mn and, indeed, the highest T_C and magnetization are observed in thinner films, typically ~ 25 nm.[9]

IV. CONCLUSION

This work addresses the lattice location and thermal stability of Mn in ferromagnetic (Ga,Mn)As doped with 1% and 5% Mn. The majority of Mn atoms have been found to substitute Ga sites, while a significant fraction occupies tetrahedral interstitial sites with As nearest neighbors.

The thermal stability of both substitutional and interstitial Mn decrease with Mn concentration, with estimated activation energies for diffusion of *interstitial Mn* at $1.6 - 2.0$ eV for 1% and $1.3 - 1.6$ eV for 5% Mn, and of *substitutional Mn* at 2.4 eV and 1.9 eV, respectively. We attribute the decrease in thermal stability for both substitutional and interstitial Mn to the interaction between the two charged defects.

These findings shed new light on our understanding of Mn self-compensation in (Ga,Mn)As. The delicate balance between interstitial and substitutional thermal stability defines the narrow temperature window in which the Curie temperature and the magnetization can be maximized. The lower limit is defined by the mobility of Mn interstitials towards passivation at the surface, whereas the higher limit is limited by the mobility of substitutional Mn, i.e. the onset of Mn segregation into secondary phases. Since the Mn concentration affects more strongly the upper limit, the optimal annealing temperature window narrows down with

increasing Mn concentration.

* lino.pereira@kuleuven.be

[1] T. Dietl and H. Ohno, "Dilute ferromagnetic semiconductors: Physics and spintronic structures," Reviews of Modern Physics **86**, 187 (2014).

[2] T. Jungwirth, J. Wunderlich, V. Novák, K. Olejník, B. L. Gallagher, R. P. Campion, K. W. Edmonds, A. W. Rushforth, A. J. Ferguson, and P. Němec, "Spin-dependent phenomena and device concepts explored in (Ga,Mn)As," Reviews of Modern Physics **86**, 855–896 (2014), 1310.1944.

[3] T. Dietl, "A ten-year perspective on dilute magnetic semiconductors and oxides," Nature Materials **9**, 965 (2010).

[4] M. Dobrowolska, K. Tivakornsasithorn, X. Liu, J. K. Furdyna, M. Berciu, K. M. Yu, and W. Walukiewicz, "Controlling the Curie temperature in (Ga,Mn)As through location of the Fermi level within the impurity band," Nature materials **11**, 444 (2012).

[5] T. Jungwirth, K. Y. Wang, J. Mašek, K. W. Edmonds, J. König, J. Sinova, M. Polini, N. A. Goncharuk, A. H. MacDonald, M. Sawicki, *et al.*, "Prospects for high temperature ferromagnetism in (Ga,Mn)As semiconductors," Physical Review B **72**, 165204 (2005).

[6] K. Yu, W. Walukiewicz, T. Wojtowicz, I. Kuryliszyn, X. Liu, Y. Sasaki, and J. Furdyna, "Effect of the location of Mn sites in ferromagnetic $Ga_{1-x}Mn_xAs$ on its Curie temperature," Physical Review B **65**, 201303 (2002).

[7] M. Wang, K. Edmonds, B. Gallagher, A. Rushforth, O. Makarovsky, A. Patanè, R. Campion, C. Foxon, V. Novak, and T. Jungwirth, "High Curie temperatures at low compensation in the ferromagnetic semiconductor (Ga,Mn)As," Physical Review B **87**, 121301 (2013).

[8] P. Němec, V. Novák, N. Tesaová, E. Rozkotová, H. Reichlová, D. Butkovičová, F. Trojánek, K. Olejník, P. Malý, R. P. Campion, *et al.*, "The essential role of carefully optimized synthesis for elucidating intrinsic material properties of (Ga,Mn)As." Nature Communications **4**, 1422 (2013).

[9] M. Wang, R. P. Campion, A. W. Rushforth, K. W. Edmonds, C. T. Foxon, and B. L. Gallagher, "Achieving high Curie temperature in (Ga,Mn)As," Applied Physics Letters **93**, 132103 (2008).

[10] K. W. Edmonds, P. Bogusławski, K. Y. Wang, R. P. Campion, S. N. Novikov, N. R. S. Farley, B. L. Gallagher, C. T. Foxon, M. Sawicki, T. Dietl, *et al.*, "Mn Interstitial Diffusion in

(Ga,Mn)As," Physical Review Letters **92**, 037201 (2004).

[11] M. Yokoyama, H. Yamaguchi, T. Ogawa, and M. Tanaka, "Zinc-blende-type MnAs nanoclusters embedded in GaAs," Journal of Applied Physics **97**, 10D317 (2005).

[12] A. Kwiatkowski, D. Wasik, M. Kamińska, R. Bożek, J. Szczytko, A. Twardowski, J. Borysiuk, J. Sadowski, and J. Gosk, "Structure and magnetism of MnAs nanocrystals embedded in GaAs as a function of post-growth annealing temperature," Journal of Applied Physics **101**, 113912 (2007).

[13] V. Baykov, P. Korzhavyi, and B. Johansson, "Diffusion of Interstitial Mn in the Dilute Magnetic Semiconductor (Ga,Mn)As: The Effect of a Charge State," Physical Review Letters **101**, 177204 (2008).

[14] J. Sadowski, J. Z. Domagala, R. Mathieu, A. Kovács, T. Kasama, R. E. Dunin-Borkowski, and T. Dietl, "Formation process and superparamagnetic properties of (Mn,Ga)As nanocrystals in GaAs fabricated by annealing of (Ga,Mn)As layers with low Mn content," Physical Review B **84**, 245306 (2011).

[15] A. Kovács, J. Sadowski, T. Kasama, M. Duchamp, and R. E. Dunin-Borkowski, "Effect of post-growth annealing on secondary phase formation in low-temperature-grown Mn-doped GaAs," Journal of Physics D: Applied Physics **46**, 145309 (2013).

[16] H. Hofsäss and G. Lindner, "Emission channeling and blocking," Physics Reports **201**, 121–183 (1991).

[17] M. R. Silva, U. Wahl, J. G. Correia, L. M. Amorim, and L. M. C. Pereira, "A versatile apparatus for on-line emission channeling experiments," Review of Scientific Instruments **84**, 073506 (2013).

[18] U. Wahl, J.G. Correia, S. Cardoso, J.G. Marques, A. Vantomme, and G. Langouche, "Electron emission channeling with position-sensitive detectors," Nuclear Instruments and Methods in Physics Research Section B: Beam Interactions with Materials and Atoms **136-138**, 744–750 (1998).

[19] S. Agostinelli, J. Allison, K. Amako, J. Apostolakis, H. Araujo, P. Dubois, M. Asai, D. Axen, S. Banerjee, G. Barrand, *et al.*, "Geant4a simulation toolkit," Nuclear Instruments and Methods in Physics Research Section A: Accelerators, Spectrometers, Detectors and Associated Equipment **506**, 250–303 (2003).

[20] J. Allison, K. Amako, J. Apostolakis, H. Araujo, P. Dubois, M. Asai, G. Barrand, R. Capra,

S. Chauvie, R. Chytracek, *et al.*, "Geant4 developments and applications," IEEE Transactions on Nuclear Science **53**, 270–278 (2006).

[21] James F. Ziegler, Jochen P. Biersack, and Matthias D. Ziegler, "SRIM, the stopping and range of ions in matter," (Lulu Press, Maryland, USA, 2009).

[22] R. P. Campion, K. W. Edmonds, L. X. Zhao, K. Y. Wang, C. T. Foxon, B. L. Gallagher, and C. R. Staddon, "The growth of GaMnAs films by molecular beam epitaxy using arsenic dimers," Journal of Crystal Growth **251**, 311–316 (2003).

[23] L. X. Zhao, C. R. Staddon, K. Y. Wang, K. W. Edmonds, R. P. Campion, B. L. Gallagher, and C. T. Foxon, "Intrinsic and extrinsic contributions to the lattice parameter of GaMnAs," Applied Physics Letters **86**, 071902 (2005).

[24] T. A. L. Lima, U. Wahl, V. Augustyns, D. J. Silva, A. Costa, K. Houben, K. W. Edmonds, B. L. Gallagher, R. P. Campion, M. J. Van Bael, *et al.*, "Identification of the interstitial Mn site in ferromagnetic (Ga,Mn)As," Applied Physics Letters **106**, 012406 (2015).

[25] "Supplementary information,".

[26] L. M. C. Pereira, U. Wahl, S. Decoster, J. G. Correia, L. M. Amorim, M. R. da Silva, J. P. Araújo, and A. Vantomme, "Stability and diffusion of interstitial and substitutional Mn in GaAs of different doping types," Physical Review B **86**, 125206 (2012).

[27] L. M. C. Pereira, U. Wahl, S. Decoster, J. G. Correia, M. R. da Silva, A. Vantomme, and J. P. Araújo, "Direct identification of interstitial Mn in heavily p-type doped GaAs and evidence of its high thermal stability," Applied Physics Letters **98**, 201905 (2011).

[28] L. M. C. Pereira, J. P. Araújo, M. J. Van Bael, K. Temst, and A. Vantomme, "Practical limits for detection of ferromagnetism using highly sensitive magnetometry techniques," Journal of Physics D: Applied Physics **44**, 215001 (2011).

[29] L. M. C. Pereira, U. Wahl, J. G. Correia, S. Decoster, L. M. Amorim, M. R. da Silva, J. P. Araújo, and A. Vantomme, "Evidence of N substitution by Mn in GaN," Physical Review B **86**, 195202 (2012).

[30] R. E. Behringer, "Number of Single, Double, and Triple Clusters in a System Containing Two Types of Atoms," The Journal of Chemical Physics **29**, 537 (1958).

[31] Raebiger, H. and Ganchenkova, M. and von Boehm, J., "Diffusion and clustering of substitutional Mn in (Ga,Mn)As," Applied Physics Letters **89**, 012505 (2006).

[32] T. Hynninen, M. Ganchenkova, H. Raebiger, and J. von Boehm, "Ferromagnetism and its

evolution during long-term annealing in (Ga,Mn)As," Physical Review B **74**, 195337 (2006).

Appendix A: Supplementary Information

1.   Re-implantation after segregation

Annealing at temperatures above $T > 400°C$ induces Mn segregation into superpara-magnetic MnAs nano-sized clusters.[14,15] Fig. S1 presents the full results of the emission channeling experiments detailed in the main text. Compared to Fig. 2, a few points are added for the experiments performed after re-implantation of ^{56}Mn probes, at annealing steps up to $T = 630°C$. The discontinuities at $450°C$ and $500°C$, for 5% Mn and 1%, respectively, correspond to measurements performed after re-implantation of ^{56}Mn at room temperature into the samples that had previously been annealed at $400°C$ and $500°C$. Note that the re-implanted samples were then annealed as indicated in the figure before proceeding with the measurements. Since Mn_s was already mobile in the annealing steps prior to the re-implantation of ^{56}Mn, the local Mn concentration has decreased with Mn_s segregation, effectively changing Mn diffusivity. Accordingly, the freshly implanted probes experienced a higher thermal stability, which ultimately led to an increase in fitted fractions.
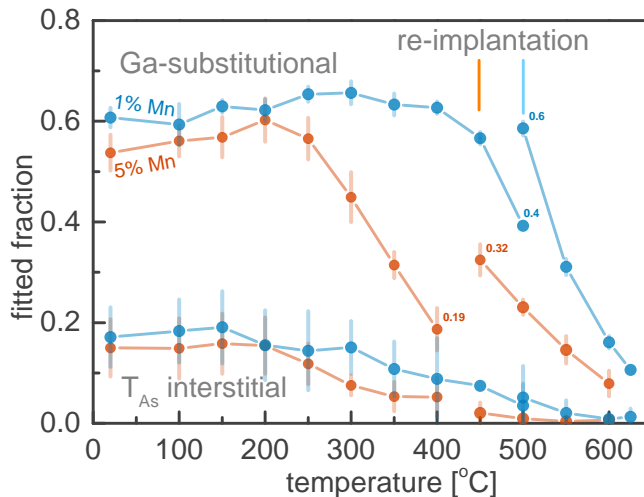

FIG. S1. Complete data from experiments on samples A and B. Fitted fractions of implanted ^{56}Mn probes in (Ga,Mn)As with different Mn concentrations. Data points beyond the indicated colored bars were taken after re-implantation of ^{56}Mn probes, in a regime where Mn_s has already started clustering, and the local Mn concentration has decreased, giving rise to discontinuities.
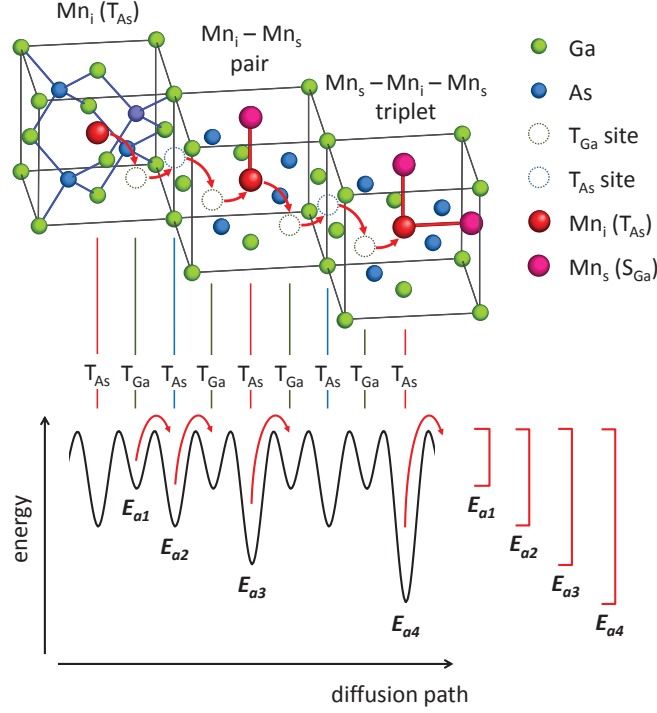
FIG. S2. (Top) Interstitial Mn as a free interstitial, in a $\mathrm{Mn_i}$-$\mathrm{Mn_s}$ pair and in a $\mathrm{Mn_s}$-$\mathrm{Mn_i}$-$\mathrm{Mn_s}$ triplet. The red arrows indicate successive $\mathrm{T_{As}} \to \mathrm{T_{Ga}} \to \mathrm{T_{As}}$ diffusion steps between the three configurations. (Bottom) Energy landscape across the same diffusion path, depicting the activation energies used in the model described in the text. This model only describes the effect of E_m and E_b on the diffusion, i.e. the Δ contributions described in the main document are not represented. In this model, E_{a2} is the same as E_m.

2. Interstitial Mn diffusion model

Within an Arrhenius model of thermally activated migration, similar to the one described in Refs. 26 and 27, the fraction $f(T, \Delta t)$ of Mn on a $\mathrm{T_{As}}$ interstitial site after an annealing step of duration Δt at a temperature T is given by:

$$f(T, \Delta t) = f_0 \exp[-\nu_0 \Delta t / N \exp(-E_a/k_B T)] \tag{A1}$$

where f_0 is the initial interstitial fraction before annealing, ν_0 is the attempt frequency, which we take as 10^{12} s^{-1}, i.e. of the order of lattice vibrations, k_B is the Boltzmann constant, and N is the average number of jumps a $\mathrm{Mn_i}$ takes before it becomes immobilized in a cluster, at the substrate or at the surface. By taking the temperature range T_D in which the initial fraction reduces to half $(f(T_D) = f_0/2)$, conservative limits for the activation energy E_a can be estimated.

20

If the diffusing Mn is considered to be a free interstitial, N includes every $\text{T}_{\text{As}} \rightarrow \text{T}_{\text{Ga}} \rightarrow \text{T}_{\text{As}}$ jump along the diffusion path. In the percent Mn regime investigated here, this assumption does not apply as a significant fraction of the interstitial impurities would be in $\text{Mn}_\text{s}\text{-Mn}_\text{i}$ or $\text{Mn}_\text{s}\text{-Mn}_\text{i}\text{-Mn}_\text{s}$ configurations. Fig. S2 demonstrates such a diffusion process detailing the required activation energies for each type of jump, E_{a1}, E_{a2}, E_{a3} and E_{a4}. Accordingly, N can be approximated as the number of jumps between trapping Mn_s centers, safely neglecting the jumps between adjacent interstitial sites, since E_{a3} and E_{a4} are a few tens of eV (E_b) higher than E_{a2}.[13] In other words, once the temperature is high enough to overcome E_{a3} and E_{a4}, the jump frequency associated with E_{a2} becomes so large that the time between E_{a3} or E_{a4} jumps is larger than that of the successive E_{a2} jumps required for Mn_i to travel between two neighboring Mn_s centers.

Statistically, in a 3–dimensional random walk, the root mean square (rms) distance from the origin after N jumps is given by $\sigma_{3,i} = \langle r^2 \rangle^{1/2} = \sqrt{N} d_i$, where d_i is the average distance between the complexes (which can be inferred from $x(1\text{Mn}_\text{s})$ and $x(2\text{Mn}_\text{s})$, introduced in the main document). Within the "thin-film" approximation, the impurity distribution is uniform along two of the three directions, and therefore only jumps in the last direction will contribute to an observable diffusivity, i.e. one third of the jumps $N/3$. This expression then reduces to $\sigma_{1,i} = \sqrt{\frac{N}{3}} d_i$. In an emission channeling experiment the implanted impurities describe a nearly Gaussian depth distribution centered at the projected range R_p. Based on the channeling/dechanneling arguments outlined in the main document, $\sigma_{1,i}$ can be approximated to the projected range of implantation R_p, resulting in $N \approx 3 \left(\frac{R_p}{d_i} \right)^2$. Since the average distance d_i depends on the trapping center ($\text{Mn}_\text{s}\text{-Mn}_\text{i}$ or $\text{Mn}_\text{s}\text{-Mn}_\text{i}\text{-Mn}_\text{s}$), different E_a values are obtained for either E_{a3}-limited or E_{a4}-limited diffusion. This estimation resulted in the following values for N: for sample A (1% Mn), $N_{\text{E}_{a4}} \approx 100$ and $N_{\text{E}_{a3}} \approx 450$, and for sample B (5% Mn), $N_{\text{E}_{a4}} \approx 500$ and $N_{\text{E}_{a3}} \approx 1300$. Since the trapping mechanism by these two predominant types of Mn complexes act simultaneously, a realistic estimate of E_a is given by the range between lowest minimum and highest maximum of the two cases, corresponding to the E_a values present in Table II from the main document.